Copyrighted Material - provided by Taylor & Francis
Correction Proof

effect of atomic orbitals on the origins of magnetism, it is worthwhile to visualize the shape of the orbitals participating in the bonding process. Spherical harmonic solutions of the angular part of the hydrogen atom problem provides the $Y_l^{m_l}(\theta,\phi)$ functions. Below we list the solution for the wavefunction

$$\psi_{nlm}(r,\theta,\phi) = R_{nl}(r)Y_l^m(\theta,\phi), \tag{11.25}$$

where the normalized radial wavefunction for the bound states of one-electron atom is written as,

$$R_{nl}(r) = -\sqrt{\left(\frac{2Z}{na_0}\right)^3 \frac{(n-l-1)!}{2n[(n+l)!]^3}} e^{-\rho/2}\rho^l L_{n+l}^{2l+1}(\rho), \tag{11.26}$$

where Z is the atomic number, a_o is the Bohr radius, $\rho = 2Zr/na_0$, and $L_{n+l}^{2l+1}(\rho)$ is the associated Laguerre polynomial. The orthonormal spherical harmonic angular wavefunction $Y_l^m(\theta,\phi)$ of degree l and order m is given by

$$Y_l^m(\theta,\phi) = (-1)^{(m+|m|)/2}\sqrt{\frac{(2l+1)}{4\pi}\frac{(l-|m|)!}{(l+|m|)!}}P_l^m(\cos\theta)e^{im\phi}, \tag{11.27}$$

where $P_l^m(\cos\theta)$ is the associated Legendre polynomial of degree l and order m. In Tables 11.10.4 and 11.10.5, we list the explicit expressions for the radial and angular part of the wavefunction up to $n = 4$. Combining the radial and the angular solutions, we obtain

$$\psi_{nlm}(r,\theta,\phi) = -\sqrt{\left(\frac{2Z}{na_0}\right)^3 \frac{(n-l-1)!}{2n[(n+l)!]^3}} e^{-\rho/2}\rho^l L_{n+l}^{2l+1}(\rho)Y_l^m(\theta,\phi), \tag{11.28}$$

with the normalization defined by

$$\int_0^\infty r^2 dr \int_0^\pi \sin\theta d\theta \int_0^{2\pi} d\phi \;\; \psi^*_{n_1 l_1 m_1}(r,\theta,\phi)\psi_{n_2 l_2 m_2}(r,\theta,\phi) = \delta_{n_1,n_2}\delta_{m_1,m_2}\delta_{l_1,l_2}. \tag{11.29}$$

In practice, to visualize the atomic orbitals we often use a spherical harmonics real basis. These real basis wavefunctions are defined in terms of the linear combination of $Y_l^{m_l}(\theta,\phi)$ functions as

$$Y_{lm} = \begin{cases} \frac{i}{\sqrt{2}}\left(Y_l^m - (-1)^m Y_l^{-m}\right) & \text{if } m < 0, \\ Y_l^0 & \text{if } m = 0, \\ \frac{1}{\sqrt{2}}\left(Y_l^{-m} + (-1)^m Y_l^m\right) & \text{if } m > 0. \end{cases} \tag{11.30}$$

Example 11.2.2.1
Write a MATLAB code to generate the radial wavefunction and radial distribution function for $n = 3$, as shown in Figure 11.2.3.
Solution
Using the exressions for the radial wavefunction from Table 11.10.4 we can write the following MATLAB code

```
%copyright by J. E Hasbun and T. Datta
% ch11_dorbital_radial.m
```

Copyrighted Material - provided by Taylor & Francis
Correction Proof


```
% Plotting the radial distribution functions
subplot(2,1,2)
plot(rho,Rthreezerosq,'o--g',rho,Rthreeonesq,'-r',rho,Rthreetwosq,'-xb',...
    'LineWidth',2);
xlabel('\rho = r/a_{o}')
ylabel('r^2 R^{2}_{nl}(\rho)')
legend('r^2 R_{30}(\rho)','r^2 R_{31}(\rho)','r^2 R_{32}(\rho)');
title('Radial distribution function')
```

Example 11.2.2.2

Using the expressions for the d orbital spherical harmonics from Table 11.10.5 and the definition of the conversion from the complex to the real basis, Equation (11.30), derive (a) the real form expressions for the five d-orbitals and (b) convert the real form to their equivalent Cartesian expressions.

Solution

For each of the choice of orbital combinations, we will first derive the real form expression and then use the conversion from polar to Cartesian form

$$x = r\sin\theta\cos\phi;\;\; y = r\sin\theta\sin\phi;\;\; z = r\cos\theta, \tag{11.31}$$

to derive the Cartesian expressions for the orbitals. We will also use the Euler identity $e^{i\theta} = \cos\theta + i\sin\theta$ to express the exponentials in terms of cosines and sines as

$$\cos\theta = \frac{e^{i\theta}+e^{-i\theta}}{2};\;\; \sin\theta = \frac{e^{i\theta}-e^{-i\theta}}{2i}. \tag{11.32}$$

1. $l = 2;\; m = -2$

$$\begin{aligned} d_{l=2}^{m=-2} &\equiv \frac{i}{\sqrt{2}}\left(Y_2^{-2} - Y_2^2\right) = \frac{i}{\sqrt{2}}\sqrt{\frac{15}{32\pi}}\sin^2\theta\left(e^{-2i\phi} - e^{2i\phi}\right), \\ &= \frac{i}{\sqrt{2}}\sqrt{\frac{15}{32\pi}}\sin^2\theta(-2i\sin 2\phi), \\ &= \sqrt{\frac{15}{16\pi}}\sin^2\theta\sin 2\phi. \end{aligned} \tag{11.33}$$

Now, to convert to Cartesian form, we write using Equation (11.31)

$$d_{l=2}^{m=-2} = 2\sqrt{\frac{15}{16\pi}}\sin^2\theta\sin\phi\cos\phi = \sqrt{\frac{15}{4\pi}}\frac{xy}{r^2} \equiv d_{xy}. \tag{11.34}$$

2. $l = 2;\; m = -1$

$$\begin{aligned} d_{l=2}^{m=-1} &\equiv \frac{i}{\sqrt{2}}\left(Y_2^{-1} + Y_2^1\right) = \frac{i}{\sqrt{2}}\sqrt{\frac{15}{8\pi}}\sin\theta\cos\theta\left(e^{-i\phi} - e^{i\phi}\right), \\ &= \frac{i}{\sqrt{2}}\sqrt{\frac{15}{8\pi}}\sin\theta\cos\theta(-2i\sin\phi), \\ &= \sqrt{\frac{15}{4\pi}}\sin\theta\sin\phi\cos\theta. \end{aligned} \tag{11.35}$$

Now, to convert to Cartesian form, we write using Equation (11.31)

$$d_{l=2}^{m=-1} = \sqrt{\frac{15}{4\pi}}\sin\theta\sin\phi\cos\theta = \sqrt{\frac{15}{4\pi}}\frac{yz}{r^2} \equiv d_{yz}. \tag{11.36}$$

Copyrighted Material - provided by Taylor & Francis
Correction Proof

3. $l = 2;\ m = 1$

$$\begin{aligned} d_{l=2}^{m=1} &= \frac{1}{\sqrt{2}}\left(Y_2^{-1} - Y_2^{1}\right) = \frac{1}{\sqrt{2}}\sqrt{\frac{15}{8\pi}}\sin\theta\cos\theta\left(e^{-i\phi} + e^{i\phi}\right), \\ &= \frac{1}{\sqrt{2}}\sqrt{\frac{15}{8\pi}}\sin\theta\cos\theta(2\cos\phi), \\ &= \sqrt{\frac{15}{4\pi}}\sin\theta\cos\phi\cos\theta. \end{aligned} \tag{11.37}$$

Now, to convert to Cartesian form, we write using Equation (11.31)

$$d_{l=2}^{m=1} = \sqrt{\frac{15}{4\pi}}\sin\theta\cos\phi\cos\theta = \sqrt{\frac{15}{4\pi}}\frac{xz}{r^2} \equiv d_{xz}. \tag{11.38}$$

4. $l = 2;\ m = 2$

$$\begin{aligned} d_{l=2}^{m=2} &\equiv \frac{1}{\sqrt{2}}\left(Y_2^{2} + Y_2^{-2}\right) = \frac{1}{\sqrt{2}}\sqrt{\frac{15}{32\pi}}\sin^2\theta\left(e^{2i\phi} + e^{-2i\phi}\right), \\ &= \frac{1}{\sqrt{2}}\sqrt{\frac{15}{32\pi}}\sin^2\theta\left(2\cos 2\phi\right), \\ &= \sqrt{\frac{15}{16\pi}}\sin^2\theta\cos 2\phi. \end{aligned} \tag{11.39}$$

Now, to convert to Cartesian form, we write using Equation (11.31)

$$\begin{aligned} d_{l=2}^{m=2} &\equiv \sqrt{\frac{15}{16\pi}}\sin^2\theta\left(2\cos^2\phi - 1\right), \\ &= \sqrt{\frac{15}{16\pi}}(\sin^2\theta\cos^2\phi - \sin^2\phi\sin^2\theta) = \sqrt{\frac{15}{16\pi}}\frac{(x^2 - y^2)}{r^2}, \\ &\equiv d_{x^2-y^2}. \end{aligned} \tag{11.40}$$

5. $l = 2;\ m = 0$

$$\begin{aligned} d_{l=2}^{m=0} \equiv Y_{20} &= \sqrt{\frac{5}{16\pi}}\left(3\cos^2\theta - 1\right), \\ &= \sqrt{\frac{5}{16\pi}}\left(3\cos^2\theta - \sin^2\theta - \cos^2\theta\right), \\ &= \sqrt{\frac{5}{16\pi}}\frac{2z^2 - x^2 - y^2}{r^2}, \\ &= \sqrt{\frac{5}{16\pi}}\frac{3z^2 - x^2 - y^2 - z^2}{r^2}, \\ &\equiv d_{3z^2-r^2}, \end{aligned} \tag{11.41}$$

where we have used $r^2 = x^2 + y^2 + z^2$ above.

In Section 11.5 you will learn how the shape of these atomic orbitals and their relative orientations play a crucial role in lifting the degeneracies of atomic levels and lead to crystal field splitting. For now, consider the MATLAB code below which generates the 3d atomic orbital. In Figure 11.2.4 we have shown the boundary surface (isosurface) representation of the five $3d$ orbitals. The boundary surface method of representing orbitals assumes that the surface encloses some substantial portion, say 90%, of the total electron density for the orbital. Consider the example shown below.

Copyrighted Material - provided by Taylor & Francis
Correction Proof

The second term can be further rewritten if we notice that

$$\vec{A}(\vec{r}_i)\cdot\vec{p}_i = \frac{B}{2}(-y_i p_{xi} + x_i p_{yi}) = \frac{1}{2}Bl_{iz} = \frac{1}{2}\vec{B}\cdot\vec{l}_i. \tag{11.86}$$

where we have used the definition of angular momentum $\vec{L} = \sum_i \vec{r}_i \times \vec{p}_i = \sum_i \vec{l}_i$. Thus Equation (11.85) becomes

$$\hat{\mathscr{H}} = \frac{1}{2m_e}\sum_{i=1}^{N_e}\vec{p}_i{}^2 + \frac{\mu_B}{\hbar}\vec{L}\cdot\vec{B} + \frac{e^2}{2m_e}\sum_{i=1}^{N_e}\vec{A}^2(\vec{r}_i). \tag{11.87}$$

Combining Equations (11.76) and (11.87) we have

$$\mathscr{H} = \frac{1}{2m_e}\sum_{i=1}^{N_e}\left[\vec{p}_i + e\vec{A}(\vec{r}_i)\right]^2 - \frac{Ze^2}{4\pi\varepsilon_o}\sum_{i=1}^{N_e}\frac{1}{r_i} + \frac{e^2}{4\pi\varepsilon_o}\sum_{i<j}\frac{1}{r_{ij}} + 2\frac{\mu_B}{\hbar}\vec{S}\cdot\vec{B}, \tag{11.88}$$

$$\mathscr{H} = \frac{1}{2m_e}\sum_{i=1}^{N_e}\left[\vec{p}_i{}^2 - \frac{Ze^2}{4\pi\varepsilon_o}\frac{1}{r_i}\right] + \frac{e^2}{4\pi\varepsilon_o}\sum_{i<j}\frac{1}{r_{ij}} + \frac{\mu_B}{\hbar}\left(\vec{L}+2\vec{S}\right)\cdot\vec{B} + \frac{e^2}{2m_e}\sum_{i=1}^{N_e}\vec{A}^2(\vec{r}_i), \tag{11.89}$$

$$\mathscr{H} = \frac{1}{2m_e}\sum_{i=1}^{N_e}\left[\vec{p}_i{}^2 - \frac{Ze^2}{4\pi\varepsilon_o}\frac{1}{r_i} + \frac{1}{2}\frac{e^2}{4\pi\varepsilon_o}\frac{1}{r_{ij}}\right] + \frac{\mu_B}{\hbar}\left(\vec{L}+2\vec{S}\right)\cdot\vec{B} + \frac{e^2B^2}{8m_e}\sum_{i=1}^{N_e}(x_i^2+y_i^2), \tag{11.90}$$

where the half factor in the third term avoids double counting. The first three terms are independent of the magnetic field and constitute the unperturbed Hamiltonian. The fourth and fifth terms are dependent on the external magnetic field. The magnetic moment can be evaluated by taking the derivative of Equation (11.90) with respect to B. This leads to

$$\vec{\mu} = -\frac{\partial\mathscr{H}}{\partial B} = -\frac{\mu_B}{\hbar}\left(\vec{L}+2\vec{S}\right) - \frac{e^2}{4m_e}\sum_{i=1}^{N_e}(x_i^2+y_i^2)\vec{B}. \tag{11.91}$$

Equation (11.91) perfectly summarizes the conceptual aspects of magnetism. The dipole moment operator is composed of two pieces – one containing the angular momentum operators and the other the effects of an external magnetic field (the diamagnetic term). In atoms, ions, or molecules which have a partially filled shell the total orbital and spin angular momentum operators do not vanish. In these cases, we have a permanent magnetic moment which can give rise to paramagnetism, ferromagnetism, antiferromagnetism, or ferrimagnetism. However, for completely filled shells the orbital and spin terms vanish since $\vec{L}=0$ and $\vec{S}=0$. In this situation, the diamagnetic term containing the effects of an induced magnetic moment become important and we have a diamagnet. Note the presence of the negative sign in front of the diamagnetic contribution. This is what causes the susceptibility to become negative. Since diamagnetism is a small effect, it is observable only when the other forms of magnetism are not present. To make further progress, we will focus solely on the diamagnetic term from Equation (11.90)

$$\mathscr{H}_{dia} = \frac{e^2B^2}{8m_e}\sum_{i=1}^{N_e}(x_i^2+y_i^2). \tag{11.92}$$

In a spherically symmetric crystal field environment

$$\langle 0|x_i^2|0\rangle = \langle 0|y_i^2|0\rangle = \langle 0|z_i^2|0\rangle = \frac{1}{3}\langle 0|r_i^2|0\rangle \equiv \frac{1}{3}\langle r_i^2\rangle, \tag{11.93}$$

where $|0\rangle$ is the ground state wave function. Utilizing Equations (11.91) and (11.93) and the fact that magnetization is the magnetic moment per unit volume we obtain an expression for the magne-

Copyrighted Material - provided by Taylor & Francis
Correction Proof

Table 11.10.4: Radial wavefunction.

n	l	Radial Wavefunction $R_{nl}(r)$
1	0	$R_{10}(r) = 2\left(\frac{Z}{a_o}\right)^{3/2} \exp(-Zr/a_o)$
2	0	$R_{20}(r) = 2\left(\frac{Z}{2a_o}\right)^{3/2}\left(1-\frac{Zr}{2a_o}\right)\exp(-Zr/2a_o)$
	1	$R_{21}(r) = \frac{1}{\sqrt{3}}\left(\frac{Z}{2a_0}\right)^{3/2}\left(\frac{Zr}{a_0}\right)\exp(-Zr/2a_0)$
3	0	$R_{30}(r) = 2\left(\frac{Z}{3a_o}\right)^{3/2}\left(1-\frac{2Zr}{3a_o}+\frac{2Z^2r^2}{27a_o^2}\right)\exp(-Zr/3a_o)$
	1	$R_{31}(r) = \frac{4\sqrt{2}}{9}\left(\frac{Z}{3a_0}\right)^{3/2}\left(\frac{Zr}{a_0}\right)\left(1-\frac{Zr}{6a_0}\right)\exp(-Zr/3a_0)$
	2	$R_{32}(r) = \frac{4}{27\sqrt{10}}\left(\frac{Z}{3a_o}\right)^{3/2}\left(\frac{Zr}{a_o}\right)^2\exp(-Zr/3a_o)$
4	0	$R_{40}(r) = 2\left(\frac{Z}{4a_o}\right)^{3/2}\left(1-\frac{3Zr}{4a_o}+\frac{Z^2r^2}{8a_o^2}-\frac{Z^3r^3}{192a_o^3}\right)\exp(-Zr/4a_o)$
	1	$R_{41}(r) = \frac{5}{2\sqrt{15}}\left(\frac{Z}{4a_o}\right)^{3/2}\left(1-\frac{Zr}{4a_o}+\frac{Z^2r^2}{80a_o^2}\right)\left(\frac{Zr}{a_o}\right)\exp(-Zr/4a_o)$
	2	$R_{42}(r) = \frac{1}{8\sqrt{5}}\left(\frac{Z}{4a_o}\right)^{3/2}\left(1-\frac{Zr}{12a_o}\right)\left(\frac{Zr}{a_o}\right)^2\exp(-Zr/4a_o)$
	3	$R_{43}(r) = \frac{1}{96\sqrt{35}}\left(\frac{Z}{4a_o}\right)^{3/2}\left(\frac{Zr}{a_o}\right)^3\exp(-Zr/4a_o)$

Copyrighted Material - provided by Taylor & Francis
Correction Proof

Table 11.10.5: Spherical Harmonics for $l = 0, 1, 2, 3, 4$.

l	m	Spherical Harmonic $Y_{lm}(\theta, \phi)$
0	0	$Y_0^0(\theta,\phi) = \frac{1}{(4\pi)^{1/2}}$
1	0	$Y_1^0(\theta,\phi) = \left(\frac{3}{4\pi}\right)^{1/2} \cos\theta$
	± 1	$Y_1^{\pm 1}(\theta,\phi) = \mp \left(\frac{3}{8\pi}\right)^{1/2} \sin\theta e^{\pm i\phi}$
2	0	$Y_2^0(\theta,\phi) = \left(\frac{5}{16\pi}\right)^{1/2} (3\cos^2\theta - 1)$
	± 1	$Y_2^{\pm 1}(\theta,\phi) = \mp \left(\frac{15}{8\pi}\right)^{1/2} \sin\theta\cos\theta e^{\pm i\phi}$
	± 2	$Y_2^{\pm 2}(\theta,\phi) = \left(\frac{15}{32\pi}\right)^{1/2} \sin^2\theta e^{\pm 2i\phi}$
3	0	$Y_3^0(\theta,\phi) = \left(\frac{7}{16\pi}\right)^{1/2} (5\cos^3\theta - 3\cos\theta)$
	± 1	$Y_3^{\pm 1}(\theta,\phi) = \mp \left(\frac{21}{64\pi}\right)^{1/2} \sin\theta(5\cos^2\theta - 1) e^{\pm i\phi}$
	± 2	$Y_3^{\pm 2}(\theta,\phi) = \left(\frac{105}{32\pi}\right)^{1/2} \sin^2\theta\cos\theta e^{\pm 2i\phi}$
	± 3	$Y_3^{\pm 3}(\theta,\phi) = \mp \left(\frac{35}{64\pi}\right)^{1/2} \sin^3\theta e^{\pm 3i\phi}$
4	0	$Y_4^0(\theta,\phi) = \left(\frac{9}{256\pi}\right)^{1/2} (35\cos^4\theta - 30\cos^2\theta + 3)$
	± 1	$Y_4^{\pm 1}(\theta,\phi) = \mp \left(\frac{45}{64\pi}\right)^{1/2} \sin\theta(7\cos^3\theta - 3\cos\theta) e^{\pm i\phi}$
	± 2	$Y_4^{\pm 2}(\theta,\phi) = \left(\frac{45}{128\pi}\right)^{1/2} \sin^2\theta(7\cos^2\theta - 1) e^{\pm 2i\phi}$
	± 3	$Y_4^{\pm 3}(\theta,\phi) = \mp \left(\frac{315}{64\pi}\right)^{1/2} \sin^3\theta\cos\theta e^{\pm 3i\phi}$
	± 4	$Y_4^{\pm 4}(\theta,\phi) = \left(\frac{315}{512\pi}\right)^{1/2} \sin^4\theta e^{\pm 4i\phi}$

11.11 Chapter 11 Exercises

11.11.1. The *Einstein−de Haas effect* experiment can be used to measure the gyromagnetic ratio and the g-factor. The basic idea behind the experiment is to use conservation of angular momentum. Consider a magnetized iron bar, in the presence of an external magnetic field, suspended from a thin elastic fiber and free to rotate. If the orientation of the magnetization is changed by reversing the direction of the external magnetic field, then the associated magnetic moments must also change direction. However, the system is isolated mechanically. Therefore the total angular momentum must be conserved. To do so, the crystal lattice must rotate to compensate for the change in angular momentum of the magnetic atoms. For this experimental set-up show that

$$\vec{M}_{bar} = \frac{g\mu_B}{\hbar}\vec{L} \tag{11.193}$$

where $\vec{M}_{bar}$ is the magnetization of the bar and $\vec{L}$ the angular momentum of the electron. By measuring $\vec{M}_{bar}$ and angular momentum $\vec{L}$ from the torsion vibrations of the string, the gyromagnetic ratio and the g-factor can be obtained. Typically, $\vec{L}$ is measured using an optical set-up based on deflection of light as shown in the experimental set-up in Figure 11.11.20.

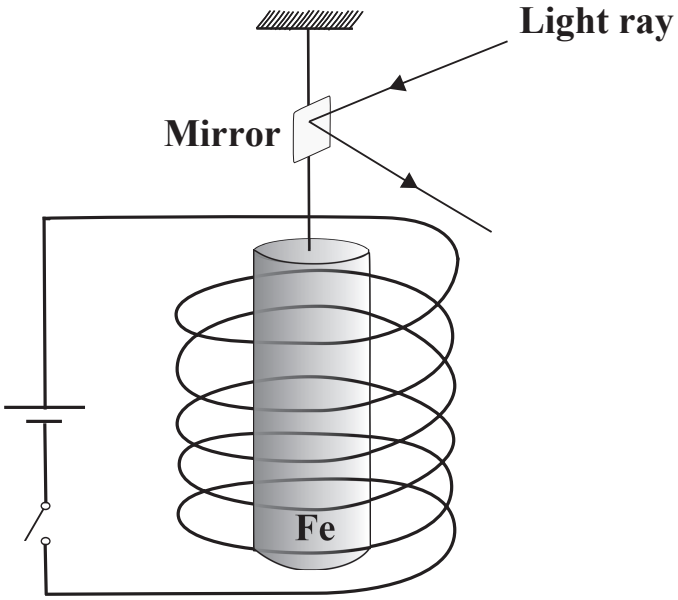

Figure 11.11.20: Einstein-de Haas effect experimental set up.

11.11.2. Using the expressions for the p orbital spherical harmonics from Table 11.10.5 and the definition of the conversion from the complex to the real basis, Equation (11.30), derive (a) the real form expressions for the three p-orbitals, (b) convert the real form to their equivalent Cartesian expressions, and (c) write a MATLAB code to generate the 2p orbitals shown in Figure 11.11.21.

Copyrighted Material - provided by Taylor & Francis
Correction Proof

11.11.4. By calculating the sum of squares of the wavefunctions given by $m_l = 0, \pm 1, \pm 2$, and ± 3 for the $4f^7 f$-orbital electron shell show that it is spherical.

11.11.5. Derive the Cartesian expressions for the spherical harmonics Y_4^4, Y_4^0, and Y_4^{-4} to show that

$$\begin{aligned} Y_4^{\pm 4} &= \sqrt{\frac{315}{512\pi}} \frac{(x \pm iy)^4}{16r^4}, \\ Y_4^0 &= \sqrt{\frac{9}{256\pi}} \frac{\left(3r^4 - 30r^2z^2 + 35z^4\right)}{r^4}. \end{aligned} \tag{11.194}$$

11.11.6. Confirm the following ground state term symbols: (a) Cu^{2+}, $^2D_{5/2}$; (b) Co^{2+}, $^4F_{9/2}$; (c) Sm^{3+}, $^6H_{5/2}$; (d) Ho^{3+}, $^5I_8$

11.11.7. Using the values of L, S, and J from Tables 11.4.1 and 11.4.2, compute the Landé g-factor and $\mu_{eff} = g\sqrt{J(J+1)}$ (in μ_B units) for the following ions (a) V^{4+}, (b) Fe^{2+}, (c) Gd^{3+}, (d) Dy^{3+}.

11.11.8. Assuming the *LS* (Russell−Saunders) coupling scheme, obtain all the possible term symbols for electrons occupying orbitals (a) $2p^1 3p^1$ and (b) $2p^5$?

11.11.9. Assuming jj-coupling scheme, obtain all the possible term symbols for electrons occupying orbitals $np^1\ nd^1$?

11.11.10. The mineral perovskite has a general stoichiometry of ABX_3 where A and B represent the cations and X is the anion. The original sample was supplied to Gustav Rose by the Chief Mines Inspector August Alexander Kammerer of the Russian Empire. Subsequently, Rose determined its physical properties and chemical composition. On the Chief Mines Inspector's suggestion Rose named the mineral after the Russian politician and mineralogist Count Lev Alekseyevich Perovski (Perovskite: Name Puzzle and German-Russian Odyssey of Discovery, Eugene Katz, *Helv. Chim. Acta* 2020, 103, e2000061). Present interest in these materials originates from their wide range of applicability ranging from solid-state ionics, sensors, fuel cells, electrooptical devices to memory devices (RAM), amplifiers, high temperature superconductors, and multiferroic materials. In Figure 11.5.11 we show a typical cubic perovskite crystal structure arrangement. An ideal cubic perovskite is realized in $SrTiO_3$ which has applications in microelectronics technology due to its high charge storage capacity (large dielectric constant). In the octahedral arrangement, eight Ti atoms reside at the cube corners, one Ti atom sits in the centre of the cube, and six oxygen atoms are located at the centre of the faces. In this problem, you will derive the crystal field potential experienced by the Ti ion at the center of the octahedra. For this purpose, consider equal point charges of value eZ, where eZ is the effective ligand charge, placed on each of the six corners of an octahedron. Choosing the origin of the Cartesian coordinates to be at the centre of the octahedron, show that the potential close to the centre is given by

$$V_{cf}^{oct} = \frac{eZ}{4\pi\varepsilon_o a}\left[6 + \frac{35}{4a^4}\left(x^4 + y^4 + z^4 - \frac{3}{5}r^4\right) + \mathcal{O}\left(\frac{r^6}{a^6}\right)\right], \tag{11.195}$$

where e is the magnitude of each charge and a is the distance between the origin and each charge. The constant term is the contribution if we treated each charge as point-like objects. The spatial part is the crystal field potential contribution.

11.11.11. The Legendre polynomials $P_l(\cos\theta))$ can be used to generate a **multipole expansion** in electrodynamics which relates the potential at point $\mathbf{r}$ created by a unit point charge located at $\mathbf{r}'$ by

$$\frac{1}{|\mathbf{r} - \mathbf{r}'|} = \sum_{l=0}^{\infty} \frac{r_<^l}{r_>^{l+1}} P_l(\cos\gamma), \tag{11.196}$$

Copyrighted Material - provided by Taylor & Francis
Correction Proof

where $r_<(r_>)$ is the smaller (larger) distance of $\mathbf{r}$ and $\mathbf{r}'$. Equation (11.196) then can be taken a step further if we utilize the addition theorem for spherical harmonic functions which can relate two coordinate vectors $\mathbf{r}$ and $\mathbf{r}'$ with spherical coordinates (r,θ,ϕ) and (r',θ',ϕ') respectively, which have an angle γ in between by

$$\frac{1}{|\mathbf{r}-\mathbf{r}'|} = \sum_{l=0}^{\infty}\sum_{m=-l}^{l} \frac{4\pi}{2l+1}\frac{r_<^l}{r_>^{l+1}} Y_l^{m*}(\theta',\phi')Y_l^m(\theta,\phi). \tag{11.197}$$

The mathematical advantage of the above equation is that it completely factorizes the

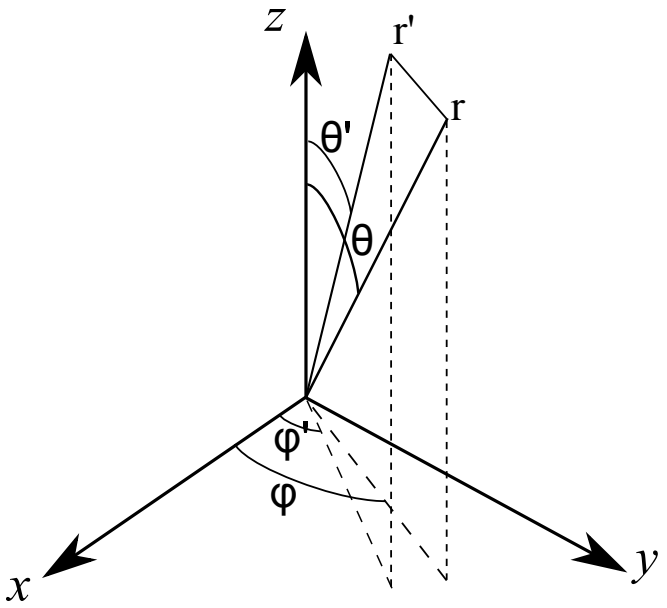

Figure 11.11.23: Spherical harmonics addition theorem.

source (primed variable) and environment (unprimed variable) charge coordinates.

(i) In Figure 11.5.11(a) an octahedral arrangement of ligand ions of charge Ze is shown surrounding a central transition metal ion where eZ is the effective ligand charge and e is the electronic charge. By considering only the $l=0$ and $l=4$ terms in Equation (11.197), show that the octahedral crystal field potential $V_{cf}^{oct}(r,\theta,\phi)$ can be written in terms of the spherical harmonics $Y_m^l(\theta,\phi)$ as

$$V_{cf}^{oct}(r,\theta,\phi) = \frac{eZ}{4\pi\varepsilon_o a}\left[6+\frac{7\sqrt{\pi}}{3}\frac{r^4}{a^4}\left\{Y_4^0+\sqrt{\frac{5}{14}}\left(Y_4^4+Y_4^{-4}\right)\right\}\right]. \tag{11.198}$$

Hint: To solve the problem, identity the spherical polar coordinates of the ligands. Note, in your problem $r_< = r$ and $r_> = a$, where a is the distance of the ligand ion along the axis in any of the three directions of the octahedral arrangement.

(ii) Show that the above form reduces to the Cartesian expression derived in Equation (11.195).

11.11.12. The ideal cubic perovskite structure in the previous problem is usually distorted resulting in an orthorhombic perovskite crystal structure, as seen for example in Lanthanum Manganite ($LaMnO_3$) – a compound which exhibits colossal magnetoresistance effect.

Copyrighted Material - provided by Taylor & Francis
Correction Proof

Show that for an orthorhombic structure the crystal field potential is given by

$$V_{cf}^{ortho} = \frac{eZ}{4\pi\varepsilon_o}\left[\frac{2}{a}+\frac{2}{b}+\frac{2}{c}+x^2\left(\frac{2}{a^3}-\frac{1}{b^3}-\frac{1}{c^3}\right)+y^2\left(\frac{2}{b^3}-\frac{1}{a^3}-\frac{1}{c^3}\right)+z^2\left(\frac{2}{c^3}-\frac{1}{a^3}-\frac{1}{b^3}\right)\right], \tag{11.199}$$

where e is the magnitude of each charge and a, b, and c is the distance between the origin and each charge. The constant term is the contribution if we treated each charge as point-like objects. The spatial part is the crystal field potential contribution.

11.11.13. As mentioned in Section 11.5, it is customary to denote the crystal field splitting value as $\Delta = 10Dq$. In this problem we will use concepts from quantum mechanics to obtain an expression for the $10Dq$ splitting. Since the crystal field splitting is an energy difference, we will compute the expectation value of the crystal field Hamiltonian (energy), in the complex basis. Beginning with Equation 11.198, derived in Exercise 11.11.11,

(a) Show that the crystal field perturbation can be written as

$$H_{m,m'} = \int d\vec{r}\,\psi^*_{nlm}(\vec{r})(eV_{cf}^{oct})\psi_{nlm} = \begin{pmatrix} \mathrm{Dq} & 0 & 0 & 0 & 5\mathrm{Dq} \\ 0 & -4\mathrm{Dq} & 0 & 0 & 0 \\ 0 & 0 & 6\mathrm{Dq} & 0 & 0 \\ 0 & 0 & 0 & -4\mathrm{Dq} & 0 \\ 5\mathrm{Dq} & 0 & 0 & 0 & \mathrm{Dq} \end{pmatrix}. \tag{11.200}$$

where $D = \frac{35e}{4a^5}$ and $q = \frac{2Ze}{105}\langle R_{32}|r^4|R_{32}\rangle$.

(b) Diagonalize the matrix in Equation 11.200 to obtain the eigenvalues. By inspecting the eigenvalues, can you explain the origin of the t_{2g} and the e_g orbital levels in Figure 11.5.11?

11.11.14. Show that the susceptibility computed in Example 11.6.0.1 is dimensionless.

11.11.15. If U is the internal energy of a statistical mechanical system at temperature T and Z the partition sum thenshow that

$$U = -\frac{d\ln Z}{d\beta}, \tag{11.201}$$

where $\beta = 1/\mathrm{T}$.

11.11.16. Derive the approximate expression for the Brillouin function given in Equation (11.112).

11.11.17. Prove the expression for the partition function Z used in Equation (11.118).

11.11.18. In Section 11.7 we introduced the idea of a two-level quantum system. Considering the splitting to be given by Δ, compute (a) the heat capacity C_V, (b) heat capacity, (c) Helmholtz-free energy, and (d) entropy for this system. For each quantity, express them in terms of suitably scaled dimensionless variable and plot the temperature variation as shown in Figure 11.11.24.

11.11.19. Derive the two-electron energy matrix, Equation (11.137), and the eigenenergy solution, Equations (11.138) and (11.139), for the singlet and triplet state. In the process of your derivation, also introduce the appropriate definition of the Coulomb integral and the Exchange integral expressions. Below are some useful hints to help you with the derivation.

(a) When considering two orbitals, we can have both the spins to be the same or different.

(b) Within different spin combinations, we could have the case where $\Psi_{\uparrow\downarrow}$ can overlap with $\Psi_{\uparrow\downarrow}$ or $\Psi_{\downarrow\uparrow}$.

Copyrighted Material - provided by Taylor & Francis
Correction Proof

Table 12.2.2: Historically important low (1−4) and high-temperature (5−23) superconductors with their critical transition temperature at ambient pressure. Material 5 is an unconventional Heavy fermion superconductor and material 6 is an organic superconductor. Cuprate high temperature superconductors are listed from 7 to 11. Material 13 is an example of alkaline fulleride superconductor. The newly discovered iron based superconductors are listed from 15 to 20.

	Material	**T_c (Kelvin)**
1.	Mercury (Hg)	4.15
2.	Aluminum (Al)	1.1
3.	Lead (Pb)	9.25
4.	Niobium (Nb)	9.25
5.	$CeCu_2Si_2$	0.7
6.	$(TMTSF)_2PF_6$ Bechgaard salt	1.1
7.	Lanthanum Barium Copper Oxide $La_{2-x}Ba_xCuO_4$ (LBCO)	35
8.	Lanthanum Strontium Copper Oxide $La_{2-x}Sr_xCuO_4$ (LSCO)	37
9.	Yttrium Barium Copper Oxide $YBa_2Cu_3O_7$ (YBCO)	91
10.	Bismuth Strontium Calcium Copper Oxide $Bi_2Sr_2CaCu_2O_{8+x}$ (BSCCO)	89
11.	Hg−Ba−Ca−Cu−O $HgBa_2Ca_2Cu_3O_8$	134
12.	Barium Bismuthate $Ba_{1-x}K_xBiO_3$	30
13.	K_3C_{60}	19
14.	MgB_2	39
15.	LaFePO	4
16.	$LaFeAsO_{0.89}F_{0.11}$	26
17.	$SmFeAsO_{0.9}F_{0.1}$	55
18.	$Ba_{1-x}K_xFe_2As_2$	38
19.	LaFeAs	18
20.	FeSe	8

2. **Persistent currents:** A sensitive test to display the absence of any resistance in a superconducting state is to generate a current in a superconducting ring and observe if there is any decay or not. Such a set-up is shown in Figure 12.2.3. For example, a metallic ring in the presence of an external magnetic field will enclose a quantized trapped flux when cooled below its superconducting transition temperature. If the field is now decreased to zero, the trapped flux remains and is maintained by a **persistent current** which flows around the ring (read Section 12.4 for a mathematical explanation). Experiments on persistent currents, also known as supercurrents, show that both the magnetic field and the persistent superconducting current is stable for several years. The supercurrent persists with zero applied voltage. The resistivity of a superconductor based on such measurements is shown to be less than 10^{-26} Ω m. Just for comparison, note that copper has a resistivity value of 1.68×10^{-8} Ωm.

Copyrighted Material - provided by Taylor & Francis
Correction Proof

this energy to the surface which corresponds to a gain in the surface energy term. Thus the first expression in Equation (12.51) has a positive contribution. On the other hand, the magnetic field contribution leads to a lowering of the condensation energy at the interface. Thus it is subtracted. The difference

$$\delta = \xi - \lambda, \tag{12.52}$$

is called the **wall-energy parameter**.

Table 12.8.5: Coherence length ξ and penetration depth λ for various types of superconductors. Data compiled from chapter 9 of *Handbook of Superconductivity* [58].

Superconductor	**T_c (Kelvin)**	**ξ (nm)**	**λ (nm)**	**κ (GL parameter)**
Al	1.18	1550	45	0.03
Sn	3.72	180	42	0.23
Nb	9.25	39	52	1.3
NbTi	9.6	3.8	130	27
UPt_3	< 1	11.1	600	54
K_3C_{60}	19.4	2.8	240	92
$La_{2-x}Sr_xCuO_4$	37	2.0	200	100
$YBa_2Cu_3O_{7-\delta}$	91	1.65	156	95
$Bi_2Sr_2CaCu_2O_{8+x}$	89	1.8	250	139

In Figure 12.8.11(a) we show the case when the coherence length builds up slowly compared to the penetration length. From the figure it is clearly evident that there is a positive free energy contribution at the surface when $\xi > \lambda$. Thus under this condition if a normal state was created inside the superconducting sample, the free energy would increase. Hence, a normal region is not possible. But, there exists another scenario where $\xi < \lambda$, in which case the free energy becomes negative as shown in Figure 12.8.11(b). Under this scenario the surface free energy is negative and the system can gain energy by allowing for the existence of the normal state within the superconducting volume. Thus by applying an external magnetic field, energy would be released when the interfaces are formed and the magnetic flux could penetrate the material. This is what gives rise to Type II superconductivity with a mixed state, see Figure 12.8.12. The former condition gives a Type I superconductor. Typical examples of Type I materials are Hg, Al, Sn, and In. Type II superconductors include Nb_3Sn, NbTi, all high T_c cuprates, fullerenes, MgB_2, and iron-based superconductors. In Table 12.8.5 we list a collection of Type I and Type II superconductors.

In most pure metals, the coherence length is quite large compared to the penetration depth. Thus, they are of Type I. However, impurities in a metal can reduce the coherence range making it substantially less than the penetration depth, thereby creating the negative surface energy possibility. Before Abrikosov's prediction, the possibility of a negative surface energy normal superconductor boundary was never appreciated. Alloys or sufficiently impure metals are thus typically Type II superconductors. The arguments presented above were mainly conceptual, derived from a purely thermodynamic perspective. A more comprehensive approach, beyond the scope of this textbook, to understanding the origins of the two different classes of superconductivity is provided by the Ginzburg-Landau theory of superconductivity. You may recall from Chapter 10, Problem 10.19, about the Landau theory of phase transition. The Ginzburg-Landau theory is a more advanced application of the same concept. The theory introduces a **Ginzburg-Landau parameter** κ defined as

$$\kappa = \lambda/\xi, \tag{12.53}$$